



# Abnormal Diastolic Hemodynamic Forces: A Link Between Right Ventricular Wall Motion, Intracardiac Flow, and Pulmonary Regurgitation in Repaired Tetralogy of Fallot

Yue-Hin Loke<sup>1,2\*†</sup>, Francesco Capuano<sup>3†</sup>, Sarah Kollar<sup>1</sup>, Merih Cibis<sup>4</sup>, Pieter Kitslaar<sup>4</sup>, Elias Balaras<sup>5</sup>, Johan H. C. Reiber<sup>4</sup>, Gianni Pedrizzetti<sup>6,7</sup> and Laura Olivieri<sup>2,8</sup>

<sup>1</sup> Department of Cardiology, Children's National Hospital, Washington, DC, United States, <sup>2</sup> 3D Cardiac Visualization Laboratory, Sheikh Zayed Institute for Pediatric Surgical Innovation, Children's National Hospital, Washington, DC, United States, <sup>3</sup> Department of Fluid Mechanics, Universitat Politècnica de Catalunya BarcelonaTech (UPC), Barcelona, Spain, <sup>4</sup> Medis Medical Imaging Systems, Leiden, Netherlands, <sup>5</sup> Laboratory for Computational Physics and Fluid Mechanics, Department of Mechanical and Aerospace Engineering, School of Engineering and Applied Science, George Washington University, Washington, DC, United States, <sup>6</sup> Department of Engineering and Architecture, University of Trieste, Trieste, Italy, <sup>7</sup> Department of Biomedical Engineering, University of California, Irvine, Irvine, CA, United States, <sup>8</sup> Department of Cardiology, UPMC Children's Hospital of Pittsburgh, Pittsburgh, PA, United States

## OPEN ACCESS

### Edited by:

Giovanni Biglino,  
University of Bristol, United Kingdom

### Reviewed by:

Jimmy Lu,  
University of Michigan, United States  
Kristen L. Billiar,  
Worcester Polytechnic Institute,  
United States

### \*Correspondence:

Yue-Hin Loke  
yloke@childrensnational.org

<sup>†</sup> These authors have contributed  
equally to this work and share first  
authorship

### Specialty section:

This article was submitted to  
Pediatric Cardiology,  
a section of the journal  
Frontiers in Cardiovascular Medicine

**Received:** 26 April 2022

**Accepted:** 20 June 2022

**Published:** 14 July 2022

### Citation:

Loke Y-H, Capuano F, Kollar S,  
Cibis M, Kitslaar P, Balaras E,  
Reiber JHC, Pedrizzetti G and  
Olivieri L (2022) Abnormal Diastolic  
Hemodynamic Forces: A Link  
Between Right Ventricular Wall  
Motion, Intracardiac Flow,  
and Pulmonary Regurgitation  
in Repaired Tetralogy of Fallot.  
*Front. Cardiovasc. Med.* 9:929470.  
doi: 10.3389/fcvm.2022.929470

**Background and Objective:** The effect of chronic pulmonary regurgitation (PR) on right ventricular (RV) dysfunction in repaired Tetralogy of Fallot (RTOF) patients is well recognized by cardiac magnetic resonance (CMR). However, the link between RV wall motion, intracardiac flow and PR has not been established. Hemodynamic force (HDF) represents the global force exchanged between intracardiac blood volume and endocardium, measurable by 4D flow or by a novel mathematical model of wall motion. In our study, we used this novel methodology to derive HDF in a cohort of RTOF patients, exclusively using routine CMR imaging.

**Methods:** RTOF patients and controls with CMR imaging were retrospectively included. Three-dimensional (3D) models of RV were segmented, including RV outflow tract (RVOT). Feature-tracking software (QStrain 2.0, Medis Medical Imaging Systems, Leiden, Netherlands) captured endocardial contours from long/short-axis cine and used to reconstruct RV wall motion. A global HDF vector was computed from the moving surface, then decomposed into amplitude/impulse of three directional components based on reference (Apical-to-Basal, Septal-to-Free Wall and Diaphragm-to-RVOT direction). HDF were compared and correlated against CMR and exercise stress test parameters. A subset of RTOF patients had 4D flow that was used to derive vorticity (for correlation) and HDF (for comparison against cine method).

**Results:** 68 RTOF patients and 20 controls were included. RTOF patients had increased diastolic HDF amplitude in all three directions ( $p < 0.05$ ). PR% correlated with Diaphragm-RVOT HDF amplitude/impulse ( $r = 0.578$ ,  $p < 0.0001$ ,  $r = 0.508$ ,  $p < 0.0001$ , respectively). RV ejection fraction modestly correlated with global HDF amplitude ( $r = 0.2916$ ,  $p = 0.031$ ).  $VO_{2-max}$  correlated with Septal-to-Free Wall HDF

impulse ( $r = 0.536$ ,  $p = 0.007$ ). Diaphragm-to-RVOT HDF correlated with RVOT vorticity ( $r = 0.4997$ ,  $p = 0.001$ ). There was no significant measurement bias between Cine-derived HDF and 4D flow-derived HDF by Bland-Altman analysis.

**Conclusion:** RTOF patients have abnormal diastolic HDF that is correlated to PR, RV function, exercise capacity and vorticity. HDF can be derived from conventional cine, and is a potential link between RV wall motion and intracardiac flow from PR in RTOF patients.

**Keywords:** Tetralogy of Fallot, hemodynamic force, 4D flow, cardiac magnetic resonance, feature tracking

## INTRODUCTION

Tetralogy of Fallot is the most common cyanotic heart disease that is surgically managed in infancy (1). Despite the excellent surgical outcomes and high survival rate in this growing population (2), adults with repaired Tetralogy of Fallot (RTOF) may suffer from long term consequences of pulmonary regurgitation (PR). These consequences include right ventricular (RV) dilation and dysfunction. Eventually, these patients may need pulmonary valve replacement (PVR) (3). Traditionally, cardiac magnetic resonance (CMR) is used to guide PVR (4). However, conventional CMR biomarkers do not clarify the direct impact of PR on RV myocardial biomechanics.

CMR studies utilizing three-dimensional (3D) spatial encoding combined with 3D velocity-encoded phase contrast (4D flow) have demonstrated that RTOF patients have significant alterations to intraventricular fluid dynamics in the RV. These alterations include abnormal vorticity, turbulent kinetic energy, viscous energy losses and hemodynamic forces (HDF) (5–8). Additionally, there are changes to ventricular geometry that correlate with RV dysfunction (9, 10). HDF in particular serves as a link between intracardiac flow and ventricular function. HDF represents the global force exchanged between blood volume and endocardium, a summation of the intraventricular pressure gradient inside the ventricular cavity (11). HDF coincides with the direction of blood flow acceleration, measurable from velocity vector fields in 4D flow by computing the material derivative term of the Navier-Stokes momentum equation (11).

To date, there has only been one 4D flow study specifically focused on HDF in RTOF patients by Sjöberg et al. in 19 RTOF patients (8). Their analysis suggests that HDF may be a biomarker for detecting cardiac dysfunction and trending changes after PVR. However, studies involving HDF are hampered by the availability of 4D flow, and its inherent limitations in spatial/temporal resolution. These limitations could potentially be addressed by deriving HDF from the wall motion instead (12). Routine CMR sequences such as cine imaging could be used to calculate HDF, via a mathematical model that relies exclusively on the position and velocity of the endocardium and the valvular planes. By combining this model with a novel reconstruction of RV kinematics, HDF could be derived irrespective of the availability of 4D flow.

Thus, the purpose of this study was to derive HDF in a retrospective cohort of RTOF patients, exclusively using

routine CMR imaging, and investigate the potential relationships between HDF, PR, and RV function.

## MATERIALS AND METHODS

This was an Institutional Review Board-approved retrospective study, involving patients who underwent a CMR study between December 2018 and August 2021. RTOF patients included those with pulmonary stenosis (TOF-PS) who underwent either transannular or infundibular patch repair, as well as those with pulmonary atresia (TOF-PA) who underwent right ventricle-to-pulmonary artery (RV-PA) conduit repair. Patients with poor imaging quality or significant stent/sternal artifact were excluded. Patients with evidence of elevated pulmonary vascular resistance (confirmed by cardiac catheterization) were also excluded. For comparison, CMR datasets from normal controls were included. Normal controls included those who underwent CMR imaging for separate clinical indication (rule out cardiomyopathy, atrial shunts or anomalous pulmonary venous drainage) and found to have normal RV size, function and pulmonary-to-systemic flow ratio ( $Q_p:Q_s$ ) < 1.2:1.

All CMR studies were performed with a Siemens 1.5T scanner. CMR data included cine imaging (long-axis and short-axis cine), contrast-enhanced magnetic resonance angiography (MRA), three-dimensional steady state free precession imaging (3D SSFP), two-dimensional phase contrast across the pulmonary valve (venc set between 2–2.5 m/s) and 4D flow. The cine acquisition sequence parameters included FOV = 270–360 × 202–270 mm, matrix = 208–256 × 156–192, TE = 1.1–1.22 ms, flip angle = 50, slice thickness = 6–8 mm, number of segments = 9–11 or 39–48 and number of acceleration factor = 2 or 4 depending on use of breath hold or motion corrected re-binning as per lab standard (13). The 4D flow acquisitions were used only for direct measurement of intracardiac vorticity and for comparison against the cine-derived HDF. The 4D flow sequence parameters included FOV = 280–480 × 140–230 mm, matrix = 160 × 77, TE = 2.19 ms, TR = 37.9–59.4 ms, flip angle = 15, slice thickness = 1.8–3 mm, venc = 2–2.5 m/s and number of reconstructed phases = 25–30. The MRA and 3D SSFP covered the entire heart with voxel size ~ 1.4 mm × 1.4 mm × 1.4 mm.

Standard clinical measurements of the RV, such as indexed end-diastolic/end-systolic volumes (RVEDVi/RVESVi), ejection fraction (RV-EF%), and pulmonary regurgitant fraction (PR%)

were obtained. For RTOF patients, electrocardiogram and cardiopulmonary exercise stress test (CPET) results within 1 years of CMR study were also collated for QRS duration, CPET parameters, including maximal oxygen consumption ( $V_{O2-max}$  and % predicted  $V_{O2-max}$ ),  $O_2$  pulse and ventilatory efficiency ( $VE/VCO_{2-max}$ ).

### 3D Modeling of Right Ventricle

3D end-diastolic models of the RV were created from MRA and 3D SSFP datasets, according to lab standard segmentation (14, 15) using commercially available software (Mimics; Materialise, Leuven, Belgium). The 3D model incorporated the three components of the RV including RV inflow, RV body/apex, and RVOT. The planes of the tricuspid/pulmonary valve annulus were carefully delineated by tagging the triangular elements and corresponding vertices on the 3D model. The RVOT was further isolated by a dividing plane orthogonal to the cranial aspect of the tricuspid annulus (parallel to the four-chamber cine plane).

### Right Ventricular Motion Reconstruction With Feature Tracking and Diffeomorphic Mapping

Long-axis and short-axis cine were used to reconstruct RV wall motion (Figure 1). Each cine was used for feature tracking analysis with QStrain V2.0 (Medis Medical Imaging Systems, Leiden, Netherlands), a semi-automated process that requires manual contour of the end-diastolic RV endocardial border to initiate tracking. In cases of insufficient tracking with apparent deviations, the RV endocardial contours were manually adjusted. The moving endocardial borders of the entire RV were then extracted and formatted as data contour points.

To create a continuous representation of RV motion, the data contour points from QStrain were used to compute diffeomorphic mappings (16) from the end-diastolic phase of the point cloud to each of the 30 phases of the cardiac cycle, as previously described using in-house MATLAB software (17, 18). Two separate sets of mappings were computed: one derived from the short-axis cine and the other from long-axis cine (i.e., three-chamber and four-chamber planes); the final transformation was then obtained by linearly superimposing the two mapping fields. The computed diffeomorphisms were applied to the segmented 3D end-diastolic model of the RV, to obtain 30 triangulated surface meshes with the same connectivity properties and with vertices correspondence (19). **Supplementary Video 1** demonstrates an example of the RV motion reconstruction. This procedure also provided the time history  $V(t)$  of the RV volume over the cardiac cycle.

### Hemodynamic Force Calculation

Historically, HDF or the global intraventricular pressure gradient was computed by integrating the material derivative of blood flow velocity over the ventricular volume, using 4D flow data. In this work, the global HDF vector  $\vec{F}(t)$  was computed according to a recently developed mathematical formalism that only requires information on the moving boundary surface that encloses

the blood volume (12). In this framework, the HDF vector is provided by

$$\vec{F}(t) = \rho \int_{S(t)} \left[ \vec{x} \left( \frac{\partial \vec{v}}{\partial t} \cdot \vec{n} \right) + v (\vec{v} \cdot \vec{n}) \right] dS \quad (1)$$

where  $S(t)$  is the RV surface, comprising both the endocardium and the valvular planes,  $\rho$  is the blood density (assumed to be equal to 1,060 kg/m<sup>3</sup>),  $\vec{x}(t)$  describes the position of the RV surface in time,  $\vec{v}(x, t)$  is the local fluid velocity at the surface, and  $\vec{n}(x, t)$  is the local unit normal vector. In order to practically apply Eq. 1 and compute the HDF for each subject from the reconstructed sets of 3D RV models, the fluid velocity needs to be defined both along the endocardium and at the valvular planes. For the closed portions of the RV surface (endocardium and closed valves), the fluid velocity is equal to the tissue velocity (an application of the no-slip condition), and evaluated numerically by central-differentiating in time the position vector of each vertex of the triangulated mesh; the same process was then used to evaluate the temporal derivative term in Eq. 1. At the open valvular planes, the following procedure was employed:

- for healthy subjects, only the pulmonary valve plane was assumed to be open in systole (resp. diastole), and the flow rate across the open portion of the RV surface was first obtained from mass conservation,  $Q(t) = - \int_{S_{closed}} \vec{v} \cdot \vec{n} dS$ , and then used to impose the velocity at the open valvular plane assuming uniform unidirectional flow,  $\vec{v}_{open} \simeq \frac{Q}{S_{open}} \vec{n}$ ;
- for RTOF patients, both the tricuspid and pulmonary valve planes were assumed to be open in diastole. The flow rate across the pulmonary valve plane was directly imposed based on the one measured by two-dimensional phase-contrast, while the flow across the tricuspid valve plane was obtained from mass conservation. The velocity on both planes was computed assuming uniform unidirectional flow.

The derived HDF vector was then divided by RV volume at each phase of the cardiac cycle to allow for proper comparison between subjects. It is worth noting that even if the derivation of Eq. 1 is formally exact, approximations are introduced in the actual calculations in terms of (i) reconstruction of RV kinematics; (ii) assumption of uniform and unidirectional flow at the valve orifices.

### Vectorization and Quantification of Diastolic Hemodynamic Force Amplitude, Impulse, and Angle

The HDF vector was decomposed into three directional components based on a reference system defined by Sjöberg et al. (8). The Apical-to-Basal direction was defined as perpendicular to the short-axis cine plane (positive amplitude is toward the base), and the Septal-to-Free Wall direction is perpendicular to both the short-axis cine plane and the three-chamber cine plane. Finally, the Diaphragm-to-RVOT direction was derived as the cross product between the other two directions (positive amplitude is

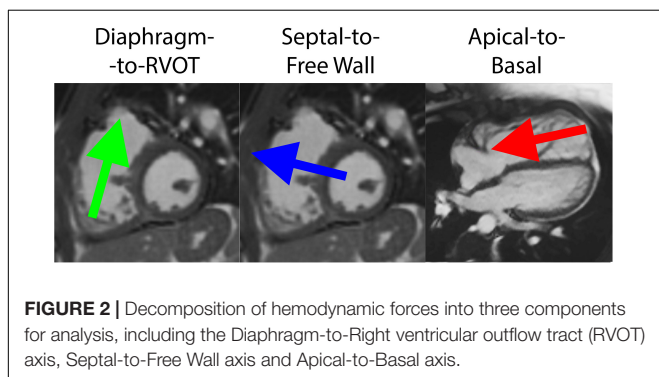
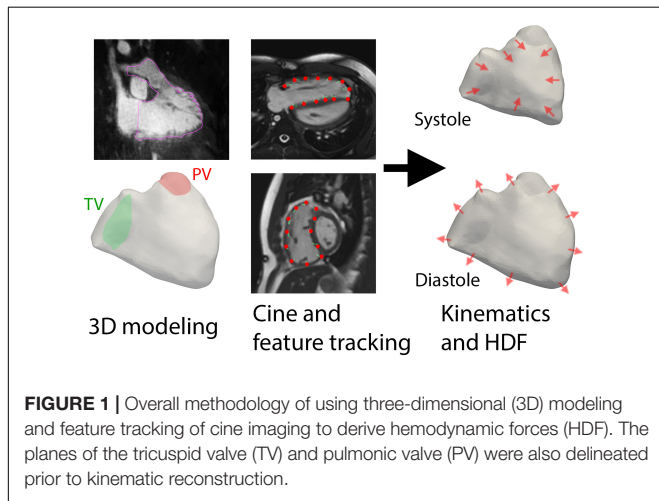
toward RVOT). The reference system is schematically illustrated in **Figure 2**.

A number of parameters were extracted from the time profile of HDF, normalized against the instantaneous RV volume: (i) the force amplitude during diastole, computed as the root mean square, normalized by the corresponding time interval; (ii) the net impulse (area under the curve) during diastole, normalized by the corresponding time interval; (iii) the angles formed by the mean diastolic force vector with the three reference axes. The amplitude and impulse were calculated for each force component as well as for the HDF module (global measurement).

### 4D Flow Quantification of Hemodynamic Force (for Comparison Only)

To validate the cine-based method for computing HDF, forces were also obtained from 4D flow datasets using the traditional approach. A segmentation mask derived from the previously described RV kinematics were used to isolate velocity vector fields within the domains of interest. After background-phase correction, the masks were further screened to remove regions of noise artifact. HDF was then calculated using the volume integral of the material time-derivative of blood velocity:

$$\vec{F}(t) = \rho \int_{V(t)} \left( \frac{\partial \vec{v}}{\partial t} + \vec{v} \cdot \nabla \vec{v} \right) d\vec{V} \quad (2)$$



and normalized against the instantaneous RV volume.

### 4D Flow Quantification of Vorticity in Right Ventricle and Right Ventricular Outflow Tract

4D flow quantification of vorticity in the total RV and RVOT was derived as part of a previous RTOF study (5). The 3D end-diastolic model of the RV and the isolated RVOT as previously described were used as a segmentation mask to isolate the velocity vector field. Vorticity was then quantified for each phase of the cardiac cycle by iTFlow (Cardioflow, Tokyo, Japan) (20). Conceptually, vorticity encodes the magnitude and the direction of local spinning motion of blood. Vorticity is defined as the curl of the velocity field,

$$\vec{\omega} = \nabla \times \vec{v}.$$

The normalized vorticity (units of 1/s) was calculated by spatially integrating the vorticity magnitude  $\|\vec{\omega}\|$  over the total RV and the RVOT, and dividing by the associated segmented volume:

$$\omega_{Total}(t) = \frac{1}{V_{Total}} \int_{V_{Total}(t)} \|\vec{\omega}\| dV$$

$$\omega_{RVOT}(t) = \frac{1}{V_{RVOT}} \int_{V_{RVOT}(t)} \|\vec{\omega}\| dV$$

The peak values within the total RV and RVOT during diastole ( $\omega_{Total-Diastole}$ ,  $\omega_{RVOT-Diastole}$ ) were collected for analysis.

### Statistical Analysis

All statistical analysis was performed with Prism 8 (Graphpad, San Diego, CA, United States). Unpaired *t*-test was used to compare between HDF parameters between RTOF patients and control groups. Subgroup analysis of RTOF patients was also performed: (#1) RTOF patients without PVR; (#2) RTOF patients with concurrent CPET parameters and (#3) RTOF patients with concurrent 4D flow data. Correlations between continuous variables were assessed using Pearson’s correlation coefficient (21). Bland-Altman analysis was used to compare percentage difference of root mean square between cine-derived HDF and 4D-flow derived HDF. The time profiles between the cine-derived HDF and 4D-flow derived HDF were compared and reported as mean correlation coefficients in each direction. Additionally, the values at each reconstructed cardiac phase were compared to identify discrepancies between the two methods. Probability values < 0.05 were considered statistically significant.

### RESULTS

Sixty-eight RTOF studies (body surface area  $1.7 \pm 0.36 \text{ m}^2$ , age  $23.4 \pm 11.2$  years) and twenty normal control studies (body surface area  $1.5 \pm 0.49 \text{ m}^2$ , age  $14 \pm 5.8$  years) were included (**Table 1**). RTOF patients consisted of 63 with TOF-PS and 5 with TOF-PA; 50 had transannular patch repair, 7 had infundibular patch repair, and 11 underwent RV-PA conduit repair. The

mean age of initial surgical repair was 1.56 months (IQR 0.31–2.0 months). 12 RTOF patients were status-post PVR at the time of CMR (Table 1). There was selection bias in that RTOF patients were older compared to control patients, albeit with similar body surface area. When compared to normal control (Table 2), the RTOF cohort had lower RV-EF%, higher RVEDVi, and moderate degree of PR% (27 ± 17%). The mean QRS duration was 143 ± 22 ms.

### Quantitative Comparison of Diastolic Hemodynamic Force Between Repaired Tetralogy of Fallot and Control

Overall comparison of diastolic HDF amplitude and impulse are summarized in Figures 3A,B. When compared to controls, RTOF patients had increased diastolic HDF amplitude in all three HDF axes and global HDF amplitude (Figure 3A). There were also alterations to the global diastolic HDF impulse, as well as the Apical-to-Basal and Septal-to-Free Wall direction (Figure 3B). For the Septal-to-Free Wall direction, this was a negative change (therefore, a larger impulse directed in the Free Wall-to-Septal

direction). The mean diastolic HDF vector in RTOF was slightly altered along the Septal-to-Free wall angle (102.3 ± 13.7 vs. 95.0 ± 10.6, *p* = 0.03), with no change in Diaphragm-to-RVOT angle (90.9 ± 21.8 vs. 84.0 ± 15.8, *p* = ns) or Apical-to-Basal angle (22.7 ± 11.7 vs. 20.7 ± 13.6, *p* = ns).

### Qualitative Comparison of Diastolic Hemodynamic Force Between Repaired Tetralogy of Fallot and Control

The alterations in diastolic HDF are elaborated in a representative RTOF patient and control of similar size/age, as demonstrated in by Figures 4A, 5. In early diastole during initial rapid filling, the RTOF patient has a larger negative amplitude in the Diaphragm-to-RVOT direction and Septal-to-Free Wall direction, likely in the same direction as PI (Figure 5). HDF then reverses into a positive amplitude along the Diaphragm-to-RVOT and Apical-to-Basal direction, corresponding to deceleration of flow. For controls, diastolic HDF predominantly is oriented along the Apical-to-Basal direction in early diastole. Finally, in diastasis (late diastole), in RTOF there is persistence of HDF in both higher RVOT-to-Diaphragm direction and Apical-to-Basal direction (likely due to continued presence of PI), whereas HDF is largely diminished in control cases by this phase of the cardiac cycle. Figure 4B demonstrates the mean value of HDF of both cohorts over time, along with their respective standard deviation, demonstrating the general alterations in the RTOF cohort.

TABLE 1 | Overall demographics.

|                             | RTOF patients<br>(n = 68)        | Controls<br>(n = 20) | <i>p</i> |
|-----------------------------|----------------------------------|----------------------|----------|
| <b>Demographics</b>         |                                  |                      |          |
| Age (years), IQR            | 23.4 (15.1–30.7)                 | 13.9 (11.7–18.4)     | 0.038    |
| Age of repair (months), IQR | 1.56 (0.31–2.0)                  |                      |          |
| Female gender               | 36 (52%)                         | 9 (45%)              |          |
| BSA (m <sup>2</sup> )       | 1.7 ± 0.36                       | 1.5 ± 0.49           | ns       |
| <b>Native anatomy</b>       |                                  |                      |          |
|                             | TOF-PS 63 (92%)<br>TOF-PA 5 (8%) |                      |          |
| <b>CMR data</b>             |                                  |                      |          |
| RV-EF%                      | 49.9% ± 6.2%                     | 54.2% ± 5.4%         | < 0.0001 |
| PR%                         | 27.5% ± 17.2%                    | 0.0 ± 0.03%          | < 0.0001 |
| RVEDVi (mL/m <sup>2</sup> ) | 137 ± 35                         | 86 ± 21              | < 0.0001 |
| RVESVi (mL/m <sup>2</sup> ) | 69 ± 21                          | 41 ± 12              | < 0.0001 |

Sixty-eight repaired Tetralogy of Fallot (RTOF) patients and twenty controls were included. There was selection bias in that RTOF patients tended to be older and larger than normal controls.

TABLE 2 | Demographics of repaired Tetralogy of Fallot (RTOF) cohort.

| Type of surgery                             | TOF-PS (n = 63) | TOF-PA (n = 5) |
|---|-----------------|----------------|
| Transannular Patch                          | 49 (78%)        | 1 (20%)        |
| Infundibular Patch                          | 7 (11%)         | 0 (0%)         |
| Right ventricle-to-pulmonary artery conduit | 7 (11%)         | 4 (80%)        |
| Subsequent pulmonary valve replacement      | 11 (16%)        | 1 (20%)        |

The cohort consisted of patients with either Tetralogy of Fallot-Pulmonary Stenosis (TOF-PS) or Tetralogy of Fallot-Pulmonary Atresia (TOF-PA). Ten patients already had pulmonary valve replacement.

### Correlations With RV-EF and PR%

Diastolic HDF correlations with RV-EF and PR% are demonstrated in Table 3 and Figure 6. Overall PR% correlated with Diaphragm-RVOT HDF amplitude/impulse/angle (*r* = 0.578, *p* < 0.0001, *r* = 0.508, *p* < 0.0001 and -0.4468, *p* = 0.0007, respectively), followed by Global HDF amplitude/impulse (*r* = 0.4431, *p* = 0.0008 and 0.423, *p* = 0.001, respectively) and Apical-to-Basal HDF amplitude/impulse (*r* = 0.294, *p* = 0.031 and *r* = 0.351, *p* = 0.009, respectively). RV-EF% modestly correlated with global HDF amplitude (0.2916, *p* = 0.031), Apical-to-Basal HDF amplitude (*r* = 0.298, *p* = 0.027) and Septum-to-Free Wall impulse (*r* = 0.284, *p* = 0.034). There were no diastolic HDF correlations with RVEDVi (HDF measurements are normalized against volume). QRS duration only modestly correlated with Diaphragm-RVOT Angle (*r* = -0.299, *p* = 0.046).

### Correlation to Exercise Capacity Testing

Among the RTOF cohort, 24 patients had CPET performed within 1.2 ± 6.1 months of CMR study. This subgroup cohort consisted of 20 with TOF-PS and 4 with TOF-PA; 20 had transannular patch, 4 had conduit repair. The mean PR% was 32 ± 17 % and mean RV-EF% was 51 ± 7%. The mean VO<sub>2-max</sub> and % predicted VO<sub>2-max</sub> was 28 ± 7 mL/kg/min and 72 ± 19%, respectively. There were no significant correlations between VO<sub>2-max</sub> and % predicted VO<sub>2-max</sub> with conventional CMR measurements of the RV (Table 4). Meanwhile, CPET parameters such as VO<sub>2-max</sub> modestly correlated with Apical-to-Basal HDF impulse (*r* = -0.408, *p* = 0.047), Septal-to-Free Wall

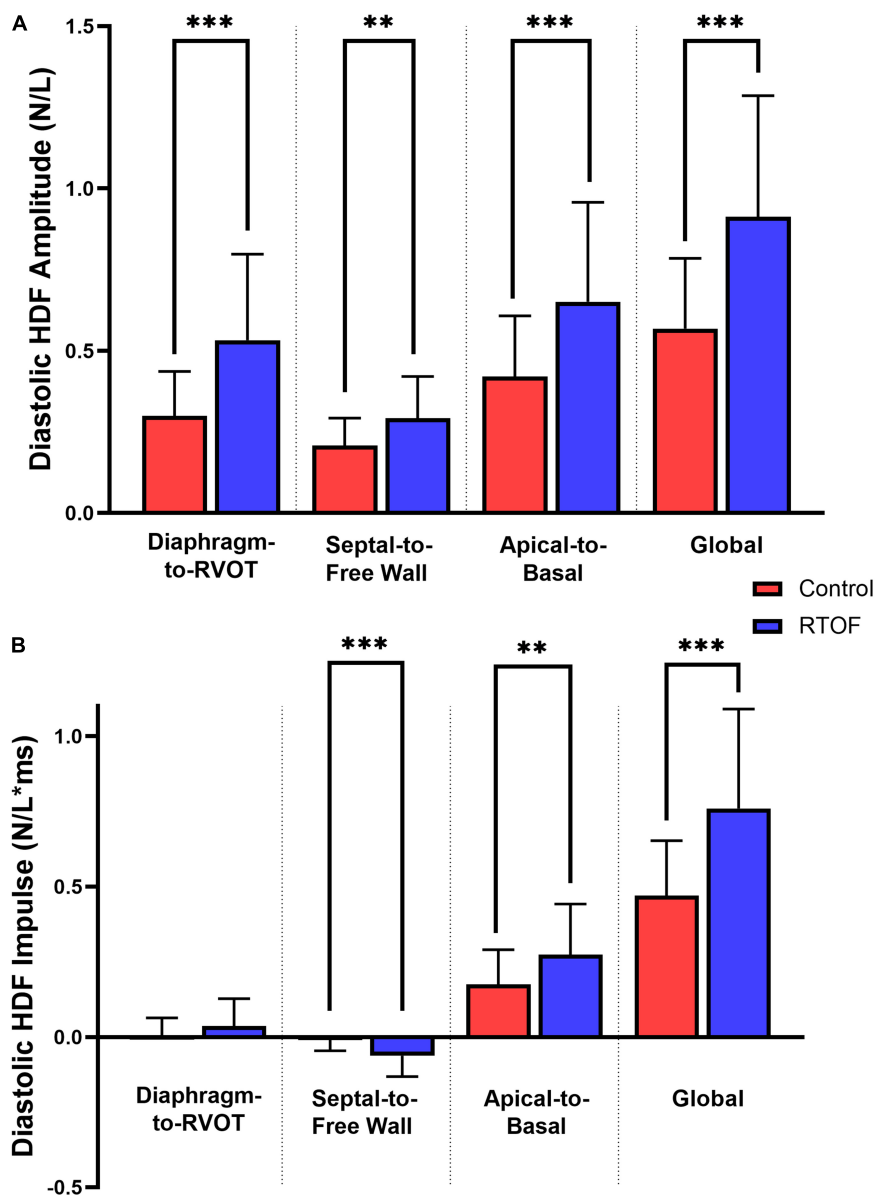


**FIGURE 3 |** Comparison of diastolic hemodynamic force (A) amplitude and (B) impulse, between repaired Tetralogy of Fallot (RTOF) patients and normal controls. \*\* $p < 0.01$ ; \*\*\* $p < 0.001$ .

HDF impulse ( $r = 0.536, p = 0.007$ ) and Global HDF Impulse ( $-0.407, p = 0.043$ ).

### Hemodynamic Force Measurements of Repaired Tetralogy of Fallot Patients With Follow-Up CMR After Pulmonary Valve Replacement

A total of 9 RTOF patients had follow-up CMR after PVR, as demonstrated in Table 5. After PVR, there was an overall decrease in PR% and RV size. There was also decrease in RVOT-to-Diaphragm HDF amplitude, increase in Septal-to-Free Wall angle and decrease in Apical-to-Basal HDF impulse. There was

also an overall decrease in the global HDF amplitude/impulse. There were otherwise no statistically significant changes in other HDF parameters.

### Correlations and Comparisons With 4D Flow

A total of 40 RTOF patients had 4D flow datasets for analysis and comparison. Total diastolic vorticity correlated with Apical-to-Basal HDF ( $r = 0.407, p = 0.009$ ) and RVOT vorticity correlated with Diaphragm-to-RVOT HDF ( $r = 0.4997, p = 0.001$ , Figure 7). The comparison of HDF derived by cine vs. 4D flow are shown in Figure 8. In general, there was underestimation of systolic

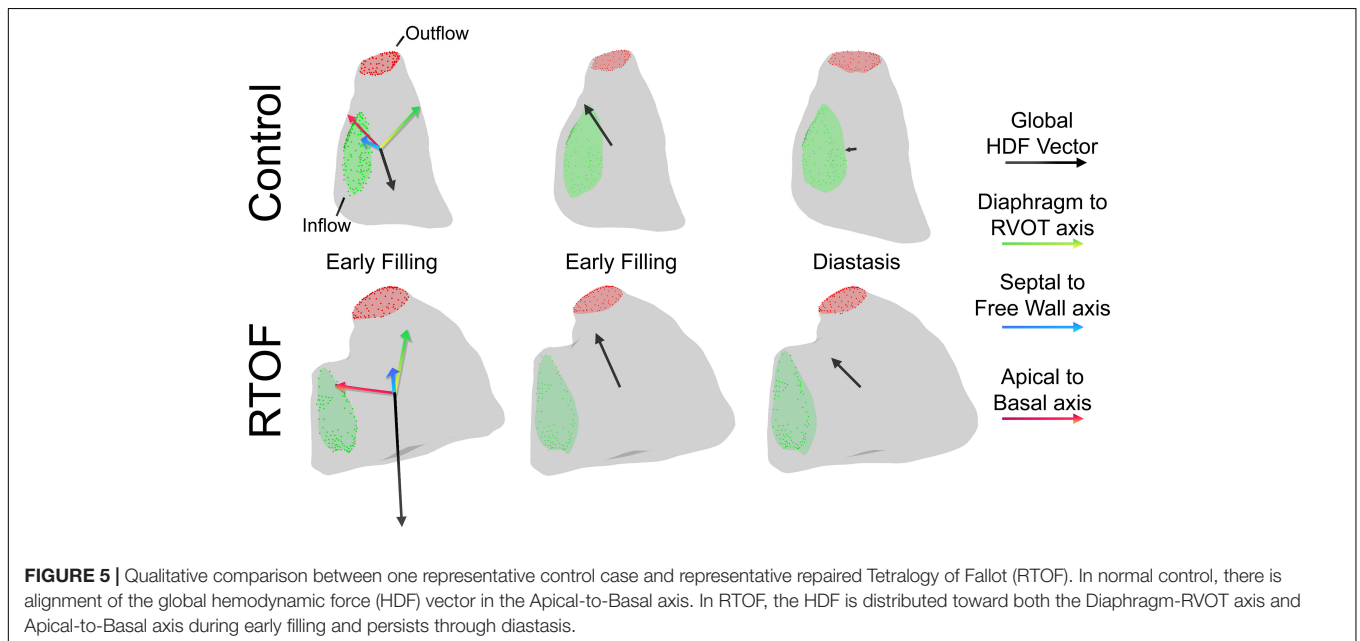
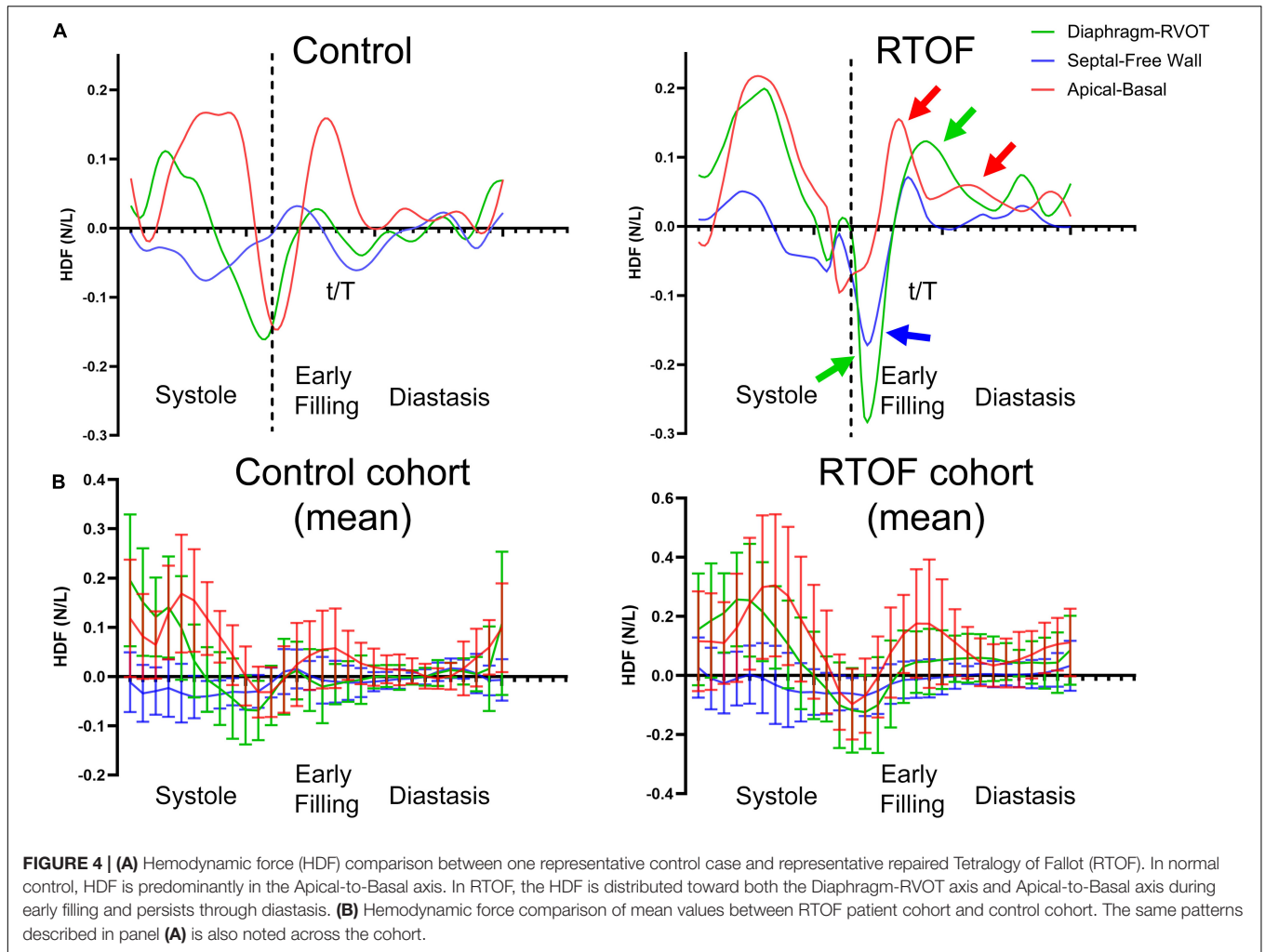


**TABLE 3 |** Subgroup correlation analysis of repaired Tetralogy of Fallot (RTOF) patients who had no subsequent pulmonary valve replacement ( $n = 56$ ).

|                                  | RV-EF%        | $p$                | PR%            | $p$                |
|----------------------------------|---------------|--------------------|----------------|--------------------|
| <b>Conventional</b>              |               |                    |                |                    |
| RV-EF%                           |               |                    | -0.210         | ns                 |
| PR%                              | -0.210        | ns                 |                |                    |
| RVEDVi (mL/m <sup>2</sup> )      | <b>-0.341</b> | <b>&lt; 0.0001</b> | <b>0.588</b>   | <b>&lt; 0.0001</b> |
| RVESVi (mL/m <sup>2</sup> )      | <b>-0.639</b> | <b>&lt; 0.0001</b> | <b>0.535</b>   | <b>&lt; 0.0001</b> |
| <b>Diastolic HDF</b>             |               |                    |                |                    |
| Diaphragm-RVOT amplitude (N/L)   | 0.145         | ns                 | <b>0.578</b>   | <b>&lt; 0.0001</b> |
| Diaphragm-RVOT impulse (N/L)     | -0.087        | ns                 | <b>0.508</b>   | <b>&lt; 0.0001</b> |
| Diaphragm-RVOT angle (deg)       | 0.1377        | ns                 | <b>-0.4468</b> | <b>0.0007</b>      |
| Septal-free wall amplitude (N/L) | <b>0.298</b>  | <b>0.027</b>       | 0.137          | ns                 |
| Septal-free wall impulse (N/L)   | 0.067         | ns                 | -0.065         | ns                 |
| Septal-free wall angle (deg)     | -0.034        | ns                 | -0.043         | ns                 |
| Apical-basal amplitude (N/L)     | <b>0.284</b>  | <b>0.034</b>       | <b>0.294</b>   | <b>0.031</b>       |
| Apical-basal impulse (N/L)       | 0.250         | ns                 | <b>0.351</b>   | <b>0.009</b>       |
| Apical-basal angle (deg)         | -0.044        | ns                 | 0.0136         | ns                 |
| Global amplitude (N/L)           | <b>0.2916</b> | <b>0.031</b>       | <b>0.4431</b>  | <b>0.0008</b>      |
| Global impulse (N/L)             | 0.2545        | ns                 | <b>0.423</b>   | <b>0.001</b>       |

*Bolded terms are statistically significant results.*

HDF along Diaphragm-RVOT direction using the cine-derived methodology, as well as slight underestimation of diastolic HDF in late diastole (during atrial systole). The difference in root mean squares between cine and 4D flow by Bland-Altman analysis was -6.72% (95% limits of agreement: -61.5 to 48.1%) for Diaphragm-to-RVOT direction, 4.97% (95% limits of agreement: -76.6 to 86.5%) for Septal-to-Free Wall direction, 1.23% (95% limits of agreement: -58.7 to 61.6%) for Apical-to-Basal direction and -3.01 (95% limits of agreement: -56.6 to 50.1%) for global HDF (Figure 9). The mean correlation coefficient between cine and 4D flow were  $0.797 \pm 0.103$  ( $p < 0.0001$ ) for Diaphragm-to-RVOT direction,  $0.535 \pm 0.22$  ( $p < 0.0001$ ) for Septal-to-Free Wall direction, and  $0.776 \pm 0.108$  ( $p < 0.0001$ ) for Apical-to-Basal direction.

## DISCUSSION

This study retrospectively analyzed conventional CMR datasets to quantify HDF in RTOF patients and normal controls. The

main findings of this study include: (#1) Diastolic HDF of the RV can be quantified by wall motion analysis instead of 4D flow; (#2) RTOF patients have alterations to diastolic HDF, particularly along the Diaphragm-to-RVOT direction and Apical-to-Basal direction; and (#3) diastolic HDF is correlated with PR, RV dysfunction, vorticity and exercise capacity. To our knowledge, this is the first RTOF study to derive HDF exclusively from conventional CMR cine imaging.

Currently, CMR metrics such as RVEDVi and RV-EF% are useful in guiding PVR therapy for RTOF, however there are still challenges in detecting subclinical dysfunction (22, 23). These conventional measurements assess RV cardiac performance in the classic framework of a pressure-volume loop, and do not account for the complex, physics-based biomechanical parameters of RV function (11). This is evident by CMR studies that demonstrate an inability for conventional measurements to predict improvement after PVR or prevent exercise intolerance (5, 22, 24–26). To date, only overt RV systolic dysfunction (a late presentation) has been predictive of low peak oxygen uptake ( $VO_{2-max}$  or % predicted  $VO_{2-max}$ ) (24).

The intraventricular and deformation parameters not traditionally considered in pressure-volume analysis are pertinent to the pathophysiology of RTOF. 4D flow studies of RTOF have demonstrated unique flow and deformation patterns that are related to PR, independent of RV size (5, 6, 27). Abnormalities in global longitudinal strain and circumferential strain, including biventricular dis-synchrony in RTOF have been well-documented (25, 28). More recently, the flow topologies by 4D flow have been directly correlated to exercise capacity (5, 29). These RTOF studies point to the concept of cardiac function as a multi-parameter, three-dimensional phenomena. In our study, we used a combination of 3D modeling and strain data to derive parameters that correlated with PR, vorticity and exercise capacity. HDF may be the potential link between PI and the altered intracardiac flow environment, abnormal RV wall motion, and clinical dysfunction in RTOF. These biomechanical markers and their physiologic effect warrant further investigation.

As a link between intracardiac flow and wall motion, HDF may have utility as an early indicator for biomechanical dysfunction in RTOF patients. Previous studies have shown that HDF represents a sensible indicator of ventricular function that may show

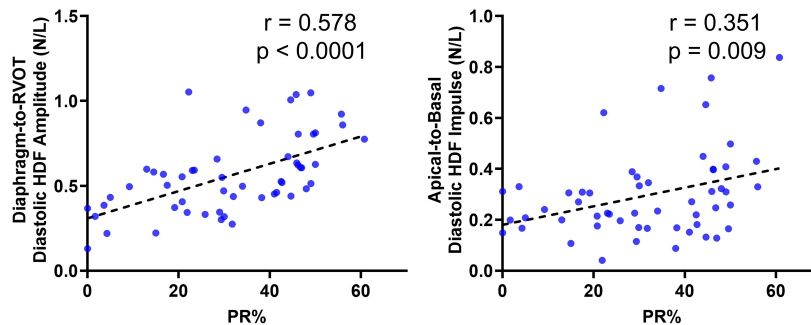


**FIGURE 6 |** Correlation of Diaphragm-to-RVOT HDF and Apical-to-basal HDF amplitude with pulmonary insufficiency in repaired tetralogy of fallot (RTOF) patients.

**TABLE 4 |** Subgroup correlation analysis of repaired Tetralogy of Fallot (RTOF) patients with exercise stress test results (n = 24).

|                                  | VO <sub>2</sub> -max | p            | % Predicted VO <sub>2</sub> -max | p            | O <sub>2</sub> pulse | p            | VE/VC <sub>O<sub>2</sub></sub> -max | p  |
|----------------------------------|----------------------|--------------|----------------------------------|--------------|----------------------|--------------|-------------------------------------|----|
| <b>Conventional</b>              |                      |              |                                  |              |                      |              |                                     |    |
| RV-EF%                           | -0.153               | ns           | -0.337                           | ns           | 0.066                | ns           | 0.110                               | ns |
| PR%                              | -0.262               | ns           | 0.204                            | ns           | 0.079                | ns           | -0.095                              | ns |
| RVEDVi (mL/m <sup>2</sup> )      | -0.103               | ns           | -0.094                           | ns           | 0.087                | ns           | -0.197                              | ns |
| RVESVi (mL/m <sup>2</sup> )      | 0.008                | ns           | -0.136                           | ns           | 0.068                | ns           | -0.178                              | ns |
| <b>Diastolic HDF</b>             |                      |              |                                  |              |                      |              |                                     |    |
| Diaphragm-RVOT amplitude (N/L)   | -0.311               | ns           | -0.148                           | ns           | -0.315               | ns           | 0.166                               | ns |
| Diaphragm-RVOT impulse (N/L)     | -0.107               | ns           | -0.185                           | ns           | -0.084               | ns           | 0.174                               | ns |
| Diaphragm-RVOT angle (deg)       | -0.154               | ns           | 0.081                            | ns           | -0.099               | ns           | -0.106                              | ns |
| Septal-free wall amplitude (N/L) | -0.158               | ns           | -0.141                           | ns           | -0.283               | ns           | -0.113                              | ns |
| Septal-free wall impulse (N/L)   | <b>0.536</b>         | <b>0.007</b> | <b>0.444</b>                     | <b>0.029</b> | <b>0.448</b>         | <b>0.028</b> | 0.253                               | ns |
| Septal-free wall angle (deg)     | <b>-0.411</b>        | <b>0.041</b> | -0.241                           | ns           | -0.167               | ns           | -0.135                              | ns |
| Apical-basal amplitude (N/L)     | -0.275               | ns           | -0.401                           | ns           | <b>-0.514</b>        | <b>0.029</b> | 0.006                               | ns |
| Apical-Basal Impulse (N/L)       | <b>-0.408</b>        | <b>0.047</b> | <b>-0.419</b>                    | <b>0.04</b>  | <b>-0.636</b>        | <b>0.005</b> | 0.012                               | ns |
| Apical-basal angle (deg)         | 0.060                | ns           | -0.170                           | ns           | -0.0752              | ns           | -0.046                              | ns |
| Global amplitude (N/L)           | -0.323               | ns           | -0.299                           | ns           | <b>-0.4686</b>       | <b>0.028</b> | 0.030                               | ns |
| Global impulse (N/L)             | <b>-0.407</b>        | <b>0.043</b> | -0.387                           | ns           | <b>-0.511</b>        | <b>0.015</b> | 0.042                               | ns |

*Bolded terms are statistically significant results.*

early alterations of ventricular function (11). HDF analysis can differentiate heart failure patients with preserved ejection fraction compared to controls with similar ejection fraction (11), reveal subclinical dysfunction due to cardiotoxicity from anthracycline chemotherapy (30), and it was the first left ventricular parameter to testify the impact of precapillary pulmonary hypertension on cardiac function (31). As HDF drives the intraventricular pressure gradient exchanged within the myocardium, stimulation of mechanoreceptors may provoke activation of intracellular pathways involved in cardiac adaptation and remodeling (32, 33). Identification of subtle kinetic dysfunction is also possible

through HDF analysis, leading to detection of mechanical abnormalities in asymptomatic patients (11). The observations of HDF in our study are in line with Sjöberg et al.'s intracardiac 4D flow analysis; furthermore, because our HDF was directly derived from RV kinematics, there is now a direct implication between altered intracardiac flow and HDF mechanics in RTOF.

The altered biomechanical environment in RTOF has been elaborated on by 4D flow, *ex-vivo* and *in-vitro* studies. In normal controls, the dominant diastolic flow in the RV is an organized, “donut”-shaped ring-vortex surrounding the tricuspid inflow, a result of longitudinal lengthening/retraction of the RV myocardium (18, 34). This vortex is passively generated instead of direct suction, which prevents the formation of large deceleration forces (along the Apical-to-Basal direction). However, in RTOF patients, the jet of PI directly collides against this vortex (5, 35), leading to an overall increase in vorticity particularly at the RVOT, as well as increased diastolic HDF in the Apical-to-Basal direction and Diaphragm-to-RVOT direction. The vortex interaction and resultant HDF likely contributes to altered mechanotransductive environment, leading to RV dilation and dysfunction (36, 37). The abnormal HDF may also contribute to the abnormal RVOT shape geometry found in RTOF (38). Furthermore, RV contractility is also affected by electromechanical dis-synchrony (39), transitioning to predominantly circumferential/radial motion and impairing the normal tricuspid inflow vortex (i.e., larger HDF in the Apical-to-Basal direction). Paradoxical recruitment of the septal wall motion (septal displacement toward the RV) likely results in the opposing Free Wall-to-Septal impulse found in our study (40, 41), and implies significant interactions with the left ventricle that lead to exercise intolerance.

Both alterations to Septal-to-Free Wall and Apical-to-Basal HDF appear to be relevant to RTOF, as these forces correlated with VO<sub>2</sub>-max, % predicted VO<sub>2</sub>-max and O<sub>2</sub> pulse in our study; better exercise capacity was in particular associated with a net diastolic impulse predominantly oriented toward the Free Wall

**TABLE 5 |** Subgroup comparison of diastolic hemodynamic force (HDF) in repaired Tetralogy of fallot (RTOF) patients, before and after pulmonary valve replacement (PVR) (n = 9).

|                                  | Before PVR           | After PVR            | p             |
|----------------------------------|----------------------|----------------------|---------------|
| <b>Conventional</b>              |                      |                      |               |
| RV-EF%                           | 47 ± 4.6             | 46 ± 5.4             | ns            |
| PR%                              | <b>36 ± 12</b>       | <b>8.6 ± 6.4</b>     | <b>0.0003</b> |
| RVEDVi (mL/m <sup>2</sup> )      | <b>178 ± 27</b>      | <b>127 ± 24</b>      | <b>0.0002</b> |
| RVESVi (mL/m <sup>2</sup> )      | <b>92 ± 14</b>       | <b>69 ± 13</b>       | <b>0.0004</b> |
| <b>Diastolic HDF</b>             |                      |                      |               |
| Diaphragm-RVOT amplitude (N/L)   | <b>0.492 ± 0.015</b> | <b>0.280 ± 0.091</b> | <b>0.0056</b> |
| Diaphragm-RVOT impulse (N/L)     | 0.051 ± 0.063        | 0.027 ± 0.060        | ns            |
| Diaphragm-RVOT angle (deg)       | 73.5 ± 8.93          | 81.5 ± 7.07          | ns            |
| Septal-free wall amplitude (N/L) | 0.277 ± 0.132        | 0.202 ± 0.078        | ns            |
| Septal-free wall impulse (N/L)   | -0.046 ± 0.043       | -0.065 ± 0.049       | ns            |
| Septal-free wall angle (deg)     | <b>88.6 ± 7.73</b>   | <b>98.5 ± 5.58</b>   | <b>0.0135</b> |
| Apical-basal amplitude (N/L)     | 0.527 ± 0.130        | 0.399 ± 0.189        | ns            |
| Apical-basal impulse (N/L)       | <b>0.246 ± 0.112</b> | <b>0.135 ± 0.058</b> | <b>0.0039</b> |
| Apical-basal angle (deg)         | 55.5 ± 9.15          | 62.8 ± 11.1          | ns            |
| Global amplitude (N/L)           | <b>0.783 ± 0.189</b> | <b>0.534 ± 0.207</b> | <b>0.017</b>  |
| Global impulse (N/L)             | <b>0.626 ± 0.161</b> | <b>0.431 ± 0.180</b> | <b>0.029</b>  |

*Bolded terms are statistically significant results.*

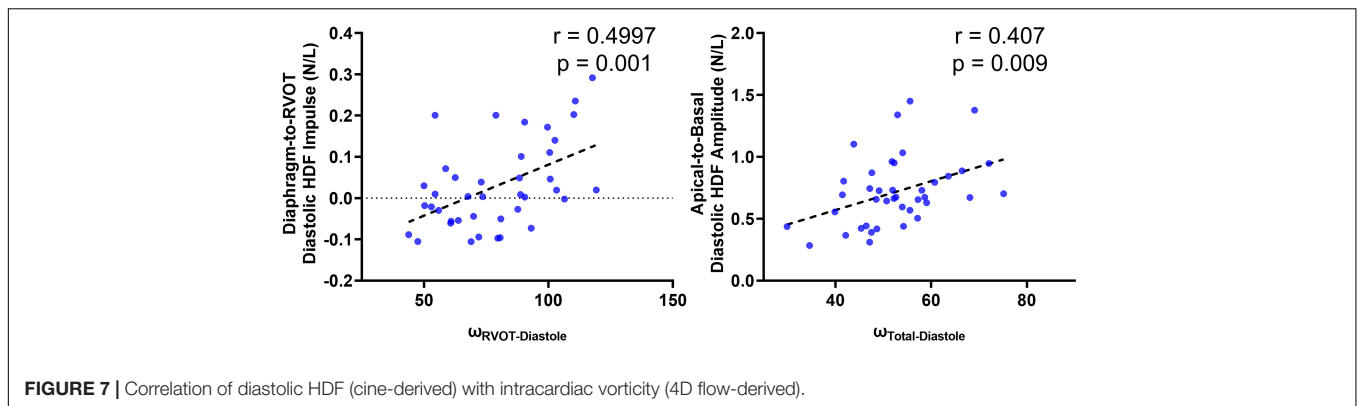


**FIGURE 7** | Correlation of diastolic HDF (cine-derived) with intracardiac vorticity (4D flow-derived).

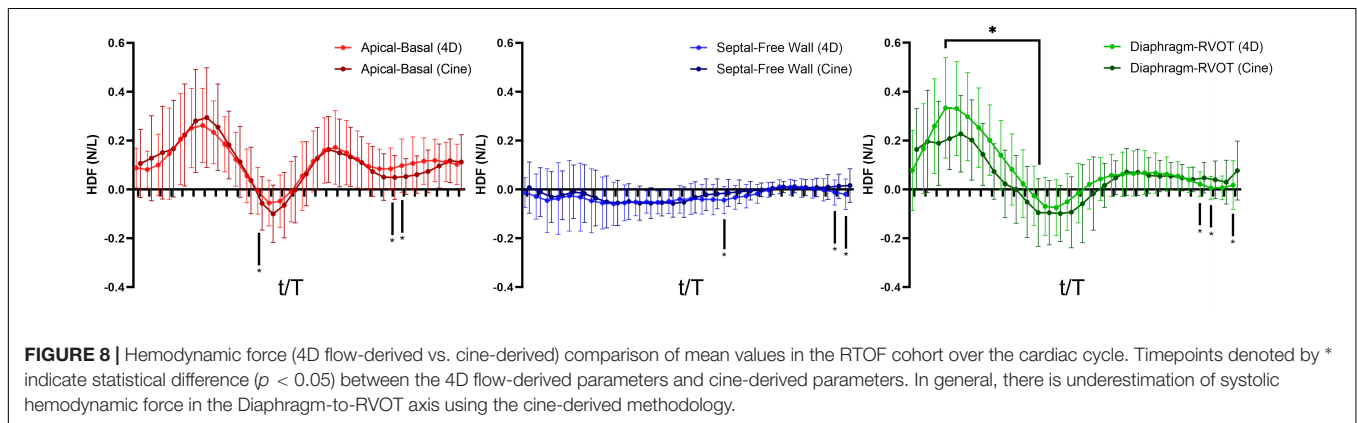


**FIGURE 8** | Hemodynamic force (4D flow-derived vs. cine-derived) comparison of mean values in the RTOF cohort over the cardiac cycle. Timepoints denoted by \* indicate statistical difference ( $p < 0.05$ ) between the 4D flow-derived parameters and cine-derived parameters. In general, there is underestimation of systolic hemodynamic force in the Diaphragm-to-RVOT axis using the cine-derived methodology.

and the apex. Previous CMR studies have not demonstrated any significant correlation between RV size and PR with exercise capacity (22, 24, 42), and exercise-based CMR studies also show no significant changes in PR%, RV size or RV-EF% during exercise (26). Thus, our results suggest that HDF is a better link between PR and exercise intolerance in RTOF, compared to PR% and RV-EF%. Since feature tracking can also be applied to real-time CMR obtained during exercise, investigation of HDF during exercise may lead to the development of deformation-based biomarkers that can detect exercise intolerance and assist in the decision of optimal timing of PVR.

Pulmonary valve replacement would likely restore the natural diastolic vortex (43), normalizing HDF and restoring RV function. However, in our study the post-PVR cohort still had persistent alterations to HDF despite the resolution of PR, similar to Sjöberg et al.'s results. This may be due to continued impairment in RV wall motion after PVR. The lack of change in Septal-to-Free wall HDF deserves attention, as this parameter best correlated with exercise capacity in our study. The effect of PVR on HDF requires further investigation, which could be performed on larger pre-and-post PVR cohorts in multicenter retrospective studies such as the INDICATOR trial (23).

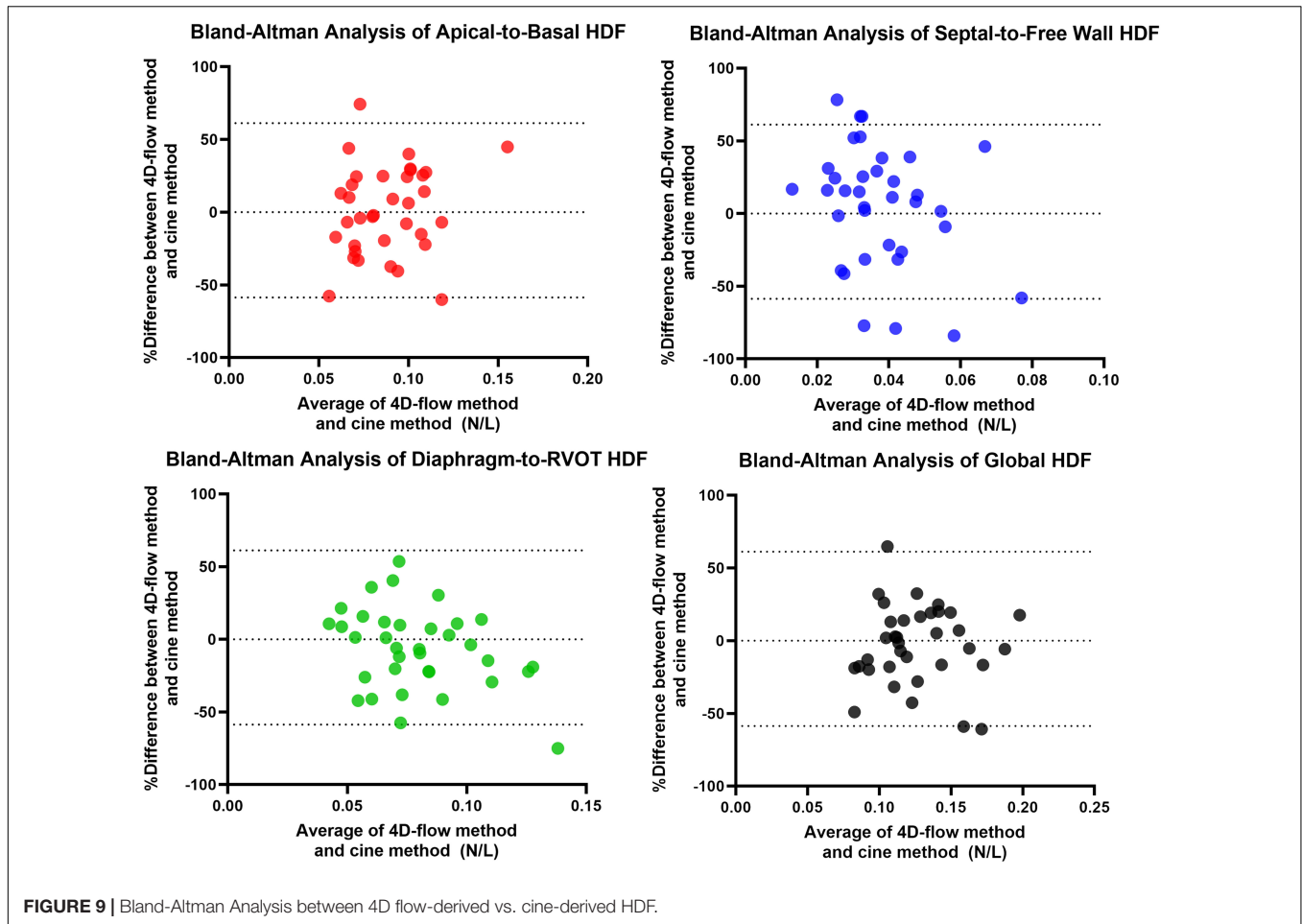
### Limitations

The study is still a single-center analysis and limited by sample size. The RTOF cohort was heterogenous in both anatomy and surgical repair, limiting the correlations observed in the study. Late gadolinium enhancement was also not routinely performed,

precluding the investigation of peri-patch fibrosis in the RVOT (44) and its effect on HDF. There was inconsistent timing of exercise stress test in RTOF patients, although the time interval between CMR and stress tests were still within recommended surveillance guidelines of RTOF patients (45) and unlikely to alter results based on previous longitudinal studies (46, 47). As the RV kinematic reconstruction is driven by imaging, the current methodology does not couple electrical propagation with mechanical contraction (48, 49), which may explain the lack of correlation between HDF and QRS duration. Most importantly, we did not interpret the systolic HDF in this cohort – this was partly due to concern that subtle deviations in feature tracking during early systole were amplified by second order effects contributing to systolic discrepancies shown in **Figure 8**.

### Future Studies

Future work will focus on in-depth simulation of intracardiac flow generated by the RV kinematics in RTOF (17, 18, 50), to further elaborate on the relationship between HDF, intracardiac flow, RV dysfunction and exercise intolerance. Further retrospective investigations using larger cohorts of pre-and-post PVR and controls are also planned. We also plan to prospectively use HDF analysis, 4D flow and computational modeling to investigate intracardiac flow in RTOF patients before-and-after PVR. We aim to further develop HDF along with intracardiac flow as clinical biomarkers to aid in timing of PVR for RTOF patients.



## CONCLUSION

In RTOF patients, there is abnormal alignment of diastolic HDF that is correlated to PR%, RV-EF%, vorticity and exercise capacity. As a global parameter, HDF can be captured by RV wall motion. HDF is a potential link between RV wall motion and intracardiac flow from PR; further studies should investigate its role in PVR timing.

## DATA AVAILABILITY STATEMENT

The raw data supporting the conclusions of this article will be made available by the authors, without undue reservation.

## ETHICS STATEMENT

The studies involving human participants were reviewed and approved by the Institutional Review Board at Children’s National Hospital (protocol Pro00013174). Written informed consent from the participants or their legal guardian/next of kin was not required to participate in

this study in accordance with the national legislation and the institutional requirements.

## AUTHOR CONTRIBUTIONS

FC and Y-HL were the primary contributors to study design, analysis of CMR measurements, interpretation of results, and writing the manuscript. SK contributed to the analysis of CMR measurements and writing the manuscript. MC, PK, and JR contributed to the analysis of CMR measurements. EB, GP, and LO contributed to the study design, interpretation of results, and writing the manuscript. All authors read and approved the final manuscript.

## FUNDING

Y-HL receives partial salary support from NIH R01 HL143468-01 and R21 HL156045. FC also received support from NIH UL1TR001876, and is a Serra Hunter Fellow. GP acknowledge partial support by Italian Ministry of Education and Research under project PRIN 2017 A889FP. This publication was supported by Award Number UL1TR001876 from the NIH National Center for Advancing Translational Sciences. This work

was also supported by institutional funding through Children's National Hospital (Board of Visitors grant) to pay for licensing of segmentation software (Mimics, Materialise).

## ACKNOWLEDGMENTS

We would like to acknowledge the support provided by all members of the iCMR program at Children's National Hospital.

## REFERENCES

- Hoffman JI, Kaplan S. The incidence of congenital heart disease. *J Am Coll Cardiol.* (2002) 39:1890–900. doi: 10.1016/S0735-1097(02)01886-7
- Bhatt AB, Foster E, Kuehl K, Alpert J, Brabeck S, Crumb S, et al. Congenital heart disease in the older adult: a scientific statement from the American Heart Association. *Circulation.* (2015) 131:1884–931. doi: 10.1161/CIR.0000000000000204
- Ferraz Cavalcanti PE, Sá MPBO, Santos CA, Esmeraldo IM, Escobar RR, de Menezes AM, et al. Pulmonary valve replacement after operative repair of tetralogy of fallot. *J Am Coll Cardiol.* (2013) 62:2227–43. doi: 10.1016/j.jacc.2013.04.107
- Geva T. Indications for pulmonary valve replacement in repaired tetralogy of fallot: the quest continues. *Circulation.* (2013) 128:1855–7. doi: 10.1161/CIRCULATIONAHA.113.005878
- Loke YH, Capuano F, Cleveland V, Mandell JG, Balaras E, Olivieri LJ. Moving beyond size: vorticity and energy loss are correlated with right ventricular dysfunction and exercise intolerance in repaired Tetralogy of Fallot. *J Cardiovasc Magn Reson.* (2021) 23:98. doi: 10.1186/s12968-021-00789-2
- Hirtler D, Garcia J, Barker AJ, Geiger J. Assessment of intracardiac flow and vorticity in the right heart of patients after repair of tetralogy of Fallot by flow-sensitive 4D MRI. *Eur Radiol.* (2016) 26:3598–607. doi: 10.1007/s00330-015-4186-1
- Fredriksson A, Trzebiatowska-Krzynska A, Dyverfeldt P, Engvall J, Ebbens T, Carlhäll CJ. Turbulent kinetic energy in the right ventricle: potential MR marker for risk stratification of adults with repaired Tetralogy of Fallot. *J Magn Reson Imaging JMRI.* (2018) 47:1043–53. doi: 10.1002/jmri.25830
- Sjöberg P, Töger J, Hedström E, Arvidsson P, Heiberg E, Arheden H, et al. Altered biventricular hemodynamic forces in patients with repaired tetralogy of Fallot and right ventricular volume overload because of pulmonary regurgitation. *Am J Physiol Heart Circ Physiol.* (2018) 315:H1691–702. doi: 10.1152/ajpheart.00330.2018
- Mauger CA, Govil S, Chabiniok R, Gilbert K, Hegde S, Hussain T, et al. Right-left ventricular shape variations in tetralogy of Fallot: associations with pulmonary regurgitation. *J Cardiovasc Magn Reson.* (2021) 23:105. doi: 10.1186/s12968-021-00780-x
- Zaidi SJ, Cossor W, Singh A, Maffesanti F, Kawaji K, Woo J, et al. Three-dimensional analysis of regional right ventricular shape and function in repaired tetralogy of Fallot using cardiovascular magnetic resonance. *Clin Imaging.* (2018) 52:106–12. doi: 10.1016/j.clinimag.2018.07.007
- Vallelonga F, Airale L, Tonti G, Argulian E, Milan A, Narula J, et al. Introduction to hemodynamic forces analysis: moving into the new frontier of cardiac deformation analysis. *J Am Heart Assoc.* (2021) 10:e023417. doi: 10.1161/JAHA.121.023417
- Pedrizetti G. On the computation of hemodynamic forces in the heart chambers. *J Biomech.* (2019) 95:109323. doi: 10.1016/j.jbiomech.2019.109323
- Merlocco A, Olivieri L, Kellman P, Xue H, Cross R. Improved workflow for quantification of right ventricular volumes using free-breathing motion corrected cine imaging. *Pediatr Cardiol.* (2019) 40:79–88. doi: 10.1007/s00246-018-1963-z
- Loke YH, Krieger A, Sable C, Olivieri L. Novel uses for three-dimensional printing in congenital heart disease. *Curr Pediatr Rep.* (2016) 4:28–34.

## SUPPLEMENTARY MATERIAL

The Supplementary Material for this article can be found online at: <https://www.frontiersin.org/articles/10.3389/fcvm.2022.929470/full#supplementary-material>

**Supplementary Video 1** | Example of Right ventricular (RV) kinematic reconstruction. This RV kinematic model incorporates wall motion derived from both short-axis (SAX) and long-axis (LAX) cine imaging using feature tracking.

- Loke YH, Harahsheh AS, Krieger A, Olivieri LJ. Usage of 3D models of tetralogy of Fallot for medical education: impact on learning congenital heart disease. *BMC Med Educ.* (2017) 17:54. doi: 10.1186/s12909-017-0889-0
- Beg MF, Miller MI, Trouvé A, Younes L. Computing large deformation metric mappings via geodesic flows of diffeomorphisms. *Int J Comput Vis.* (2005) 61:139–57. doi: 10.1023/B:VISI.0000043755.93987.aa
- Capuano F, Loke YH, Olivieri L, Balaras E. Computational modeling of right ventricle flow dynamics in congenital heart disease. In: García-Villalba M, Kuerten H, Salvetti MV editors. *Direct and Large Eddy Simulation XII [Internet]*. (Vol. 27), Cham: Springer International Publishing (2020). p. 477–83. doi: 10.1007/978-3-030-42822-8\_63
- Loke YH, Capuano F, Balaras E, Olivieri LJ. Computational modeling of right intracardiac motion and intracardiac flow in repaired tetralogy of fallot. *Cardiovasc Eng Technol.* (2022) 13:41–54. doi: 10.1007/s13239-021-00558-3
- Biffi B, Bruse JL, Zuluaga MA, Ntsinjana HN, Taylor AM, Schievano S. Investigating cardiac motion patterns using synthetic high-resolution 3d cardiovascular magnetic resonance images and statistical shape analysis. *Front Pediatr.* (2017) 5:34. doi: 10.3389/fped.2017.00034/full
- Nakaji K, Itatani K, Tamaki N, Morichi H, Nakanishi N, Takigami M, et al. Assessment of biventricular hemodynamics and energy dynamics using lumen-tracking 4D flow MRI without contrast medium. *J Cardiol.* (2021) 78:79–87. doi: 10.1016/j.jjcc.2021.01.004
- Chan YH. Biostatistics 104: correlational analysis. *Singapore Med J.* (2003) 44:614–9.
- Ta HT, Critser PJ, Alsaied T, Germann J, Powell AW, Redington AN, et al. Modified ventricular global function index correlates with exercise capacity in repaired tetralogy of fallot. *J Am Heart Assoc.* (2020) 9:e016308. doi: 10.1161/JAHA.120.016308
- Tretter JT, Redington AN. Risk factors and biomarkers of poor outcomes: time to throw out right ventricular volumes in repaired tetralogy of fallot? Lessons from the INDICATOR cohort. *Circulation.* (2018) 138:2116–8. doi: 10.1161/CIRCULATIONAHA.118.037000
- Rashid I, Mahmood A, Ismail TF, O'Meagher S, Kutty S, Celermajer D, et al. Right ventricular systolic dysfunction but not dilatation correlates with prognostically significant reductions in exercise capacity in repaired Tetralogy of Fallot. *Eur Heart J Cardiovasc Imaging.* (2020) 21:906–13. doi: 10.1093/ehjci/jez245
- Kalaitzidis P, Orwat S, Kempny A, Robert R, Peters B, Sarikouch S, et al. Biventricular dyssynchrony on cardiac magnetic resonance imaging and its correlation with myocardial deformation, ventricular function and objective exercise capacity in patients with repaired tetralogy of Fallot. *Int J Cardiol.* (2018) 264:53–7. doi: 10.1016/j.ijcard.2018.04.005
- Steinmetz M, Stümpfig T, Seehase M, Schuster A, Kowallick J, Müller M, et al. Impaired exercise tolerance in repaired tetralogy of fallot is associated with impaired biventricular contractile reserve: an exercise-stress real-time cardiovascular magnetic resonance study. *Circ Cardiovasc Imaging.* (2021) 14:e011823. doi: 10.1161/CIRCIMAGING.120.011823
- Elsayed A, Mauger CA, Ferdian E, Gilbert K, Scadeng M, Occleshaw CJ, et al. Right ventricular flow vorticity relationships with biventricular shape in adult tetralogy of fallot. *Front Cardiovasc Med.* (2022) 8:806107. doi: 10.3389/fcvm.2021.806107
- Berganza FM, de Alba CG, Özcelik N, Adebó D. Cardiac magnetic resonance feature tracking biventricular two-dimensional and three-dimensional strains to evaluate ventricular function in children after repaired tetralogy of fallot

- as compared with healthy children. *Pediatr Cardiol.* (2017) 38:566–74. doi: 10.1007/s00246-016-1549-6
29. Zhao X, Hu L, Leng S, Tan RS, Chai P, Bryant JA, et al. Ventricular flow analysis and its association with exertional capacity in repaired tetralogy of Fallot: 4D flow cardiovascular magnetic resonance study. *J Cardiovasc Magn Reson.* (2022) 24:4. doi: 10.1186/s12968-021-00832-2
  30. van der Velde N, Janus CPM, Bowen DJ, Hassing HC, Kardys I, van Leeuwen FE, et al. Detection of subclinical cardiovascular disease by cardiovascular magnetic resonance in lymphoma survivors. *JACC CardioOncology.* (2021) 3:695–706. doi: 10.1016/j.jacc.2021.09.015
  31. Vos JL, Leiner T, van Dijk APJ, Pedrizzetti G, Alenezi F, Rodwell L, et al. Cardiovascular magnetic resonance-derived left ventricular intraventricular pressure gradients among patients with precapillary pulmonary hypertension. *Eur Heart J Cardiovasc Imaging.* (2022) jeab294. doi: 10.1093/ehjci/jeab294 (https://pubmed.ncbi.nlm.nih.gov/34993533/) [Epub ahead of print].
  32. Filomena D, Cimino S, Monosilio S, Galea N, Mancuso G, Francone M, et al. Impact of intraventricular haemodynamic forces misalignment on left ventricular remodelling after myocardial infarction. *ESC Heart Fail.* (2021) 9:496–505. doi: 10.1002/ehf2.13719
  33. Pasipoularides A. Diastolic filling vortex forces and cardiac adaptations: probing the epigenetic nexus. *Hell J Cardiol HJC Hell Kardiologike Epiteores.* (2012) 53:458–69.
  34. Pasipoularides A, Shu M, Shah A, Womack MS, Glower DD. Diastolic right ventricular filling vortex in normal and volume overload states. *Am J Physiol-Heart Circ Physiol.* (2003) 284:H1064–72. doi: 10.1152/ajpheart.00804.2002
  35. Mikhail A, Labbio GD, Darwish A, Kadem L. How pulmonary valve regurgitation after tetralogy of fallot repair changes the flow dynamics in the right ventricle: an in vitro study. *Med Eng Phys.* (2020) 83:48–55. doi: 10.1016/j.medengphy.2020.07.014
  36. Pasipoularides A. Mechanotransduction mechanisms for intraventricular diastolic vortex forces and myocardial deformations: part 1. *J Cardiovasc Transl Res.* (2015) 8:76–87. doi: 10.1007/s12265-015-9611-y
  37. Pasipoularides A. Mechanotransduction mechanisms for intraventricular diastolic vortex forces and myocardial deformations: part 2. *J Cardiovasc Transl Res.* (2015) 8:293–318.
  38. Shen WC, Chen CA, Chang CI, Chen YS, Huang SC, Wu MH, et al. Outflow tract geometries are associated with adverse outcome indicators in repaired tetralogy of Fallot. *J Thorac Cardiovasc Surg.* (2020) 162:196–205.
  39. Lumens J, Fan CS, Walmsley J, Yim D, Manlhiot C, Dragulescu A, et al. Relative impact of right ventricular electromechanical dyssynchrony versus pulmonary regurgitation on right ventricular dysfunction and exercise intolerance in patients after repair of tetralogy of fallot. *J Am Heart Assoc.* (2019) 8:e010903. doi: 10.1161/JAHA.118.010903
  40. Kollar S, Klaus B, Capuano F, Salazar O, Olivieri L, Loke YH. Septal segmental displacement is related to right ventricular remodeling and intracardiac vorticity in repaired tetralogy of fallot patients. In: *Virtual Research Poster presented at the Society for Cardiovascular Magnetic Resonance 2022 Scientific Sessions.* Fort Lauderdale, FL (2022).
  41. Kollar SE, Klas B, Mosha MH, Channing AT, Walling S, Toro-Salazar OH. Abstract 13159: effect of pulmonary valve replacement on function and right ventricular volume by cardiac magnetic resonance imaging in patients with repaired tetralogy of fallot. *Circulation.* (2019) 140(Suppl. 1):A13159–13159.
  42. Avesani M, Borrelli N, Krupickova S, Sabatino J, Donne GD, Ibrahim A, et al. Echocardiography and cardiac magnetic resonance in children with repaired tetralogy of fallot: new insights in cardiac mechanics and exercise capacity. *Int J Cardiol.* (2020) 321:144–9. doi: 10.1016/j.ijcard.2020.07.026
  43. Loke YH, Yildiran I, Capuano F, Olivieri L, Balaras I. Computational modeling of the right ventricular in repaired tetralogy of fallot, before and after pulmonary valve replacement. *J Am Coll Cardiol.* (2022) 79:1367.
  44. Ghonim S, Ernst S, Keegan J, Giannakidis A, Spadotto V, Voges I, et al. Three-dimensional late gadolinium enhancement cardiovascular magnetic resonance predicts inducibility of ventricular tachycardia in adults with repaired tetralogy of fallot. *Circ Arrhythm Electrophysiol.* (2020) 13:e008321. doi: 10.1161/CIRCEP.119.008321
  45. Stout KK, Daniels CJ, Abouhosn JA, Bozkurt B, Broberg CS, Colman JM, et al. 2018 AHA/ACC guideline for the management of adults with congenital heart disease: a report of the American college of cardiology/American heart association task force on clinical practice guidelines. *Circulation.* (2019) 139:e698–800. doi: 10.1161/CIR.0000000000000603
  46. Bhat M, Mercer-Rosa L, Fogel MA, Harris MA, Paridon SM, McBride MG, et al. Longitudinal changes in adolescents with TOF: implications for care. *Eur Heart J Cardiovasc Imaging.* (2017) 18:356–63. doi: 10.1093/ehjci/jew272
  47. Kipps AK, Graham DA, Harrild DM, Lewis E, Powell AJ, Rhodes J. Longitudinal exercise capacity of patients with repaired tetralogy of fallot. *Am J Cardiol.* (2011) 108:99–105.
  48. Shade JK, Cartoski MJ, Nikolov P, Prakosa A, Doshi A, Binka E, et al. Ventricular arrhythmia risk prediction in repaired Tetralogy of Fallot using personalized computational cardiac models. *Heart Rhythm.* (2020) 17:408–14. doi: 10.1016/j.hrthm.2019.10.002
  49. Moss R, Wülfers EM, Schuler S, Loewe A, Seemann GA. Fully-coupled electro-mechanical whole-heart computational model: influence of cardiac contraction on the ECG. *Front Physiol.* (2021) 12:778872. doi: 10.3389/fphys.2021.778872
  50. Capuano F, Romano L, Loke YH, Dellegrottaglie S, Notorio M, Cocchia R, et al. P1449 CMR-driven computational modeling of right ventricular flow dynamics. *Eur Heart J Cardiovasc Imaging.* (2020) 21(Suppl. 1):jez319.877.
- Author Disclaimer:** The contents are solely the responsibility of the authors and do not necessarily represent the official views of the National Center for Advancing Translational Sciences or the National Institutes of Health.
- Conflict of Interest:** MC, PK, and JR were employed by Medis Medical Imaging Systems.
- The remaining authors declare that the research was conducted in the absence of any commercial or financial relationships that could be construed as a potential conflict of interest.
- Publisher's Note:** All claims expressed in this article are solely those of the authors and do not necessarily represent those of their affiliated organizations, or those of the publisher, the editors and the reviewers. Any product that may be evaluated in this article, or claim that may be made by its manufacturer, is not guaranteed or endorsed by the publisher.
- Copyright © 2022 Loke, Capuano, Kollar, Cibis, Kitslaar, Balaras, Reiber, Pedrizzetti and Olivieri. This is an open-access article distributed under the terms of the Creative Commons Attribution License (CC BY). The use, distribution or reproduction in other forums is permitted, provided the original author(s) and the copyright owner(s) are credited and that the original publication in this journal is cited, in accordance with accepted academic practice. No use, distribution or reproduction is permitted which does not comply with these terms.